Journal of Crystal Growth 425 (2015) 393–397

Contents lists available at ScienceDirect

Journal of Crystal Growth

journal homepage: www.elsevier.com/locate/jcrysgro

InGaN pn-junctions grown by PA-MBE: Material characterization and fabrication of nanocolumn electroluminescent devices

I. Gherasoiu [a,*], K.M. Yu [b,c], L. Reichertz [b], W. Walukiewicz [b]

[a] State University of New York Polytechnic Institute, Utica, NY, United States
[b] Material Sciences Division, Lawrence Berkeley National Laboratory, Berkeley, CA, United States
[c] Department of Physics and Materials Science, City University of Hong Kong, Kowloon, Hong Kong

ARTICLE INFO

Communicated by A. Brown
Available online 12 February 2015

Keywords:
A1. Doping
A1. Nanostructures
A3. Molecular beam epitaxy
B1. Nitrides
B3. Light emitting diodes

ABSTRACT

PN junctions are basic building blocks of many electronic devices and their performance depends on the structural properties of the component layers and on the type and the amount of the doping impurities incorporated.

Magnesium is the common p-type dopant for nitride semiconductors while silicon and more recently germanium are the n-dopants of choice.

In this paper, therefore we analyze the quantitative limits for Mg and Ge incorporation on GaN and InGaN with high In content. We also discuss the challenges posed by the growth and characterization of InGaN pn-junctions and we discuss the properties of large area, long wavelength nanocolumn LEDs grown on silicon (1 1 1) by PA-MBE.

1. Introduction

Nitride semiconductors containing indium have a direct band gap spanning from 0.65 eV (InN) to 3.4 eV (GaN) [1]. This large range in the band gap of InGaN alloys could allow the fabrication of full-spectrum solar cells as well as long wavelength LEDs.

For device applications, controllable doping of InGaN is essential and requires the reduction of electron background due to native and/or crystalline defects, especially in alloys with high indium content. For this reason, the InGaN alloys have been subject of sustained work targeting the synthesis of layers with high crystalline quality and high indium fraction ($>30\%$) [2,3].

Even when high quality GaN substrates are available their usefulness for the growth of thick or high indium fraction ($x>30\%$) $In_xGa_{1-x}N$ layers is limited by the formation of misfit dislocations at the InGaN/GaN interface.

As a result, the operation of the nitride devices is typically hampered by the presence of threading dislocations originating at these interfaces. One approach suggested for the mitigation of the dislocation effects and for the control of the indium segregation in InGaN alloys is the growth of nano-structured devices [4–6].

In this work we report a detailed study on Mg and Ge doping of InGaN and describe the fabrication of large area green and yellow InGaN nanocolumn LEDs on Si (1 1 1) substrates. Finally we discuss the mechanism responsible for the reduction of the electroluminescence intensity of these nanocolumn devices.

2. Materials and methods

The films were grown using 2 in. insulating GaN-on-sapphire templates and the growth of GaN and InGaN films was initiated by depositing 200 nm of nominally un-doped GaN, using a production-style plasma-assisted molecular beam epitaxy system (PA-MBE). The samples of GaN doped with magnesium were grown at 605° C. All InGaN films were grown at a substrate temperature of 545° C, except where indicate differently, using the same indium flux and have a thickness of 300 nm. Mg cell temperature was increased such that the equivalent beam pressure (BEP) at the sample surface ranged from $\sim 1\times10^{-9}$ Torr to 1.6×10^{-7} Torr. The light emitting diode structures have been grown on 4 in. p-type silicon (1 1 1) wafers. The typical structure is Si(1 1 1)/AlN/n-GaN/n-InGaN/p-InGaN/p-GaN and the estimated thickness of the Ga containing layers (n-GaN/NC-InGaN/p-GaN) is 300 nm/850 nm–1000 nm/160 nm. During the growth of the nanocolumns In and Ga fluxes were set for BEP 3×10^{-7} Torr, and 4×10^{-8} Torr respectively while the Nitrogen plasma had a total flow of 18 sccm with an approximate BEP of 1.4×10^{-4} Torr. The growth temperature for these samples, at the substrate surface, was between 515°C and 525°C.

The composition and the thickness of the films were evaluated by Rutherford backscattering spectrometry (RBS) and secondary ion mass spectrometry (SIMS), while crystallinity of the film was

* Corresponding author.
E-mail address: gherasi@sunyit.edu (I. Gherasoiu).

http://dx.doi.org/10.1016/j.jcrysgro.2015.02.015
0022-0248/

evaluated using the ion channeling. Electrical properties of the films were determined using Hall effect and electrochemical capacitance voltage (ECV) measurements . Finally, optical emission from photoluminescence (PL) and the electroluminescence (EL) were measured using an OceanOptics spectrometer.

3. Results and discussion

The properties of Mg doped GaN and InGaN films with indium fraction up to 40% have been investigated. Normalized ion channeling yield, χ has been used as a measure of the crystalline quality. The effect of magnesium incorporation on the structural quality of GaN films is presented in Fig. 1. The decrease of the channeling yield at surface, in comparison with the channeling yield at 500 nm, suggests the improvement of crystal structure with the progression of growth. The comparison also indicates that the differences in doping behavior that are seen in the mid region (p&n) of the graph in Fig. 1 are not caused by crystal defects whether buried or at surface.

Fig. 1 suggests that the crystalline perfection of the Mg doped GaN degrades as the Mg concentration in the film increases. Drastic degradation of the film crystallinity occurs at Mg concentrations of $\sim 6–7 \times 10^{20}/cm^3$. The plot also indicates that, for the experimental conditions described, hole conduction can be achieved and maintained up to a magnesium concentration of $\sim 2 \times 10^{20}/cm^3$. This is in agreement with our previous report [7] that the p-type conduction domain is followed by a sudden transition to n-type conduction ensued around a Mg concentration of $7 \times 10^{20}/cm^3$. The inclusion of new SIMS measurements in this data set suggests that between $2 \times 10^{20}/cm^3$ and $\sim 6–7 \times 10^{20}/cm^3$ the material conductivity, as measured by Hall method, can be dominated by either electrons or holes as can be seen in Fig. 1.

The crystlline quality of the n-type samples in this region, as suggested by the normalized ion channeling, appears to be similar to p-type samples that have incorporated less Mg and therefore does not seem to be the cause of the electron conduction. The evolution of GaN crystallinity for one of these samples is presented in Fig. 2.

At the interface with the insulating template, the film exhibits increased lattice disorder that is reflected in the relative larger ion channeling yield. As the growth advances the channeling yield decreases in a linear fashion and the trend does not change with the arrival of Mg at the growth surface. The mobility associated with hole carriers has been found to be correlated with the Mg

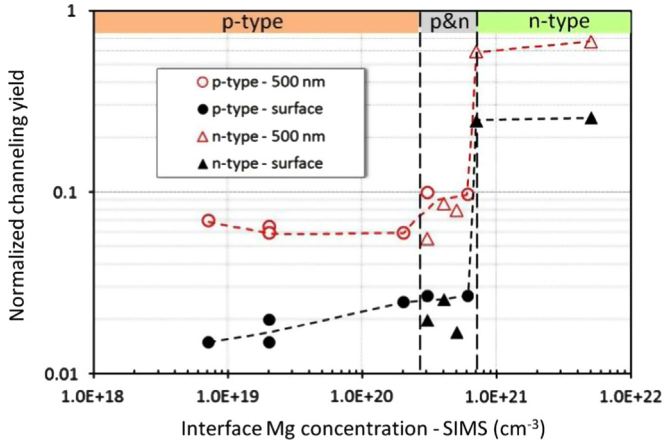

Fig. 1. Effect of magnesium incorporation in GaN as expressed by the ion channeling yield. Mg concentration has been determined by SIMS. Low values of the channeling yield are associated whit a low density of structural defects while higher scattering rates result due lattice imperfections.

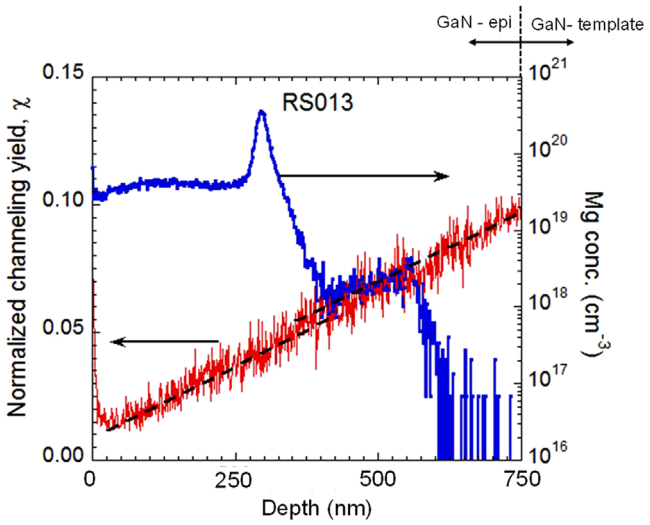

Fig. 2. Evolution of the GaN crystalline quality as expressed by the ion channeling yield during the film growth and magnesium doping. Mg concen-tration has been determined by SIMS.

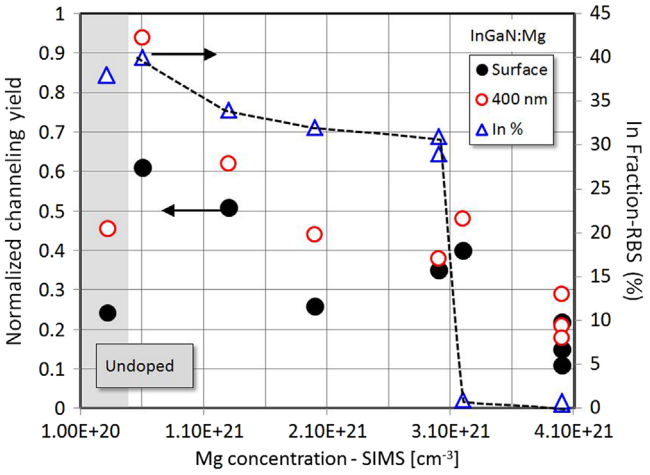

Fig. 3. Effect of magnesium incorporation on the $In_xGa_{1-x}N$ indium fraction and crystalline quality, as reflected by the ion channeling yield.

concentration. The hole mobility can be modeled, with a good correlation coefficient ($R^2 = 0.885$), by a power law of the impurity density with a negative scaling coefficient ($\alpha = -5.1$). The correlation between the hole mobility and the Mg concentration is an indication of the origin of the p-type conduction with Mg ionization. The measurements show that high hole mobility (10–12 $cm^2/V\,s$) is associated with the lower Mg concentration ($2 \times 10^{19}/cm^3$) while the hole mobility decreases ($\sim 2\ cm^2/V\,s$) with the increase of the magnesium concentration.

For the n-type samples, the electron mobility does not correlate well with the increase of the Mg concentration suggesting that extended defects originating in the Mg doping process rather than point defects are responsible for the generation of the conduction electrons. The large density of Mg in this growth regime could hamper the nitrogen incorporation leading to the formation of nitrogen vacancies (V_N) and the formation of Mg_{Ga}–V_N complexes [8,9]. The electron mobilities are in the range from 50 $cm^2/V\,s$ ($5 \times 10^{18}/cm^3$-Hall density) to 152 $cm^2/V\,s$ ($1 \times 10^{18}/cm^3$-Hall density) for Mg concentrations larger than $3 \times 10^{20}/cm^3$. InGaN films with indium fractions up to 40% as estimated by RBS have been grown and doped with Mg and Ge. Channeling yield has been used to evaluate the crystalline

quality of the films, with and without Mg doping. The evolution of the yield with the increase of the Mg concentration is presented in Fig. 3.

The incorporation of indium determines the degradation of the InGaN film crystalline quality when compared with GaN, the ion channeling yield being about one order of magnitude larger in the case of InGaN films, whether measured at surface (0.2–0.26) or 400 nm below (0.37–0.46). The channeling yield therefore cannot be used to accurately represent the effect of Mg incorporation. In this case the magnesium incorporation limit has been determined based on the competition between In and Mg for the group III lattice site. This substitution is characterized by a threshold with respect to indium incorporation, as can be seen in Fig. 3.

The determination of the electrical characteristics of the InGaN films doped with Mg is challenging for a couple of reasons. On one hand, Mg-doped layers are typically grown on top of thin un-doped InGaN films that exhibit native n-type conductivity. The relatively large defect density of the InGaN films with high indium fraction ($>20\%$) ensures that the metal contacts used for the fabrication of the Hall samples have a high likelihood to contact both layers, p-type and n-type. This results in Hall measurements where the mobility and carrier concentration reflect predominantly the n-type layer, since the contacts with this material are usually ohmic.

On the other hand, for InGaN films with indium fraction larger than 35% the Fermi level becomes pinned above the conduction band edge and as a result electrons accumulate at the surface. The conductivity measurement of such films will reflect mostly the surface electron accumulation, obscuring to a large extent the properties of the carriers in the bulk.

Germanium has been used as n-type dopant for both GaN and InGaN layers. For these layers, we have determined the electron concentration and mobility using Hall measurements. For both GaN and InGaN we have found electrons concentrations in the range from $1\times10^{18}/\mathrm{cm}^3$ to $7\times10^{20}/\mathrm{cm}^3$. At low electron concentration the mobility in the films reaches the maximum while with increasing carrier concentration, associated with increased Ge incorporation, the electron mobility saturates and converges for both films to values around 40 cm^2/V-s.

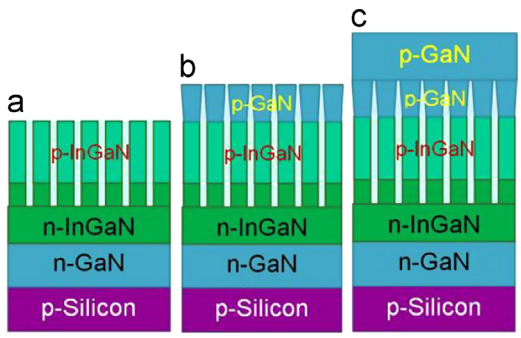

Fig. 4. Schematic of the main growth steps of the nanocolumn LED. (a) Nucleation and development of the InGaN nanocolumns, (b) start of the nanocolumn coalescence, (c) fully coalesced GaN:Mg cap layer.

The goal of analyzing the doping characteristics of the GaN and InGaN layers was to allow the growth of p–n junction devices with optimized properties. The presence of dislocations leads to a decrease of the device performance, as represented by the external quantum efficiency (EQE). Another factor contributing to the low operation efficiency of the nitride devices is the charge polarization that leads to the quantum confined Stark effect (QCSE).

A possible solution attempting to overcome these detrimental properties concerns the growth of nanocolumn based devices. The nanocolumns growth can eliminate or reduce the density of misfit dislocations [4], and suppress the effect of the polarization field if the p-n junctions are fabricated along the radial direction that coincides with the direction of non-polar III-nitride planes.

In this context, the catalyst-free growth appears as an attractive alternative that allows the growth of high crystalline quality nitrides with no need for substrate patterning. In Fig. 4, the schematic of the structures grown is presented. The goal of the growth was three fold: (1) to nucleate and grow InGaN nanocolumns, (2) to form pn-junctions in InGaN by doping the upper side of the columns with Mg, and (3) to grow a continuous p-type GaN cap layer that could isolate the junction region from the device surface. The accurate evolution stage of the nanostructures cannot be evaluated in-situ. Therefore, to reach the goals of InGaN nanocolumn growth and of a continuous p-GaN cap-layer, a series of samples have been grown under identical growth conditions. For these samples the growth was stopped at essential stages, as indicated by RHEED and schematically represented in Fig. 4, to study the surface morphology. The surface of the samples has been imaged by SEM and the pictures obtained for each of these 3 stages are presented in Fig. 5.

Fabrication of nanocolumns using a catalyst-free approach resulted in an average surface density, regardless of the cross-sectional size column density of $\sim 23\ \mu\mathrm{m}^{-2}$ and the nanocolumns occupy approximately 76% of the growth plane surface. The estimated diameters of the nanocolumns range from $\sim$100 nm up to $\sim$300 nm. The majority (64%) of them have cross-sections that can be approximated by circles with diameters between 150 nm and 200 nm and if the diameters up to 300 nm are included the proportion of nanocolumns in this range reaches 90%.

The predominance of the diameters between 150 nm and 200 nm suggests that the lateral growth is limited and most of the material is deposited along the *c*-axis of the nanocolumn which is expected for the nitrogen-rich PA-MBE growth. This observation is in agreement with the model proposed by Foxon et al. [10]. For the case of our structures another mechanism is obvious. As the diameter of the nanocolumns increases, the space available between the columns decreases to the point where the arrival of the precursors is impeded by a shadowing effect.

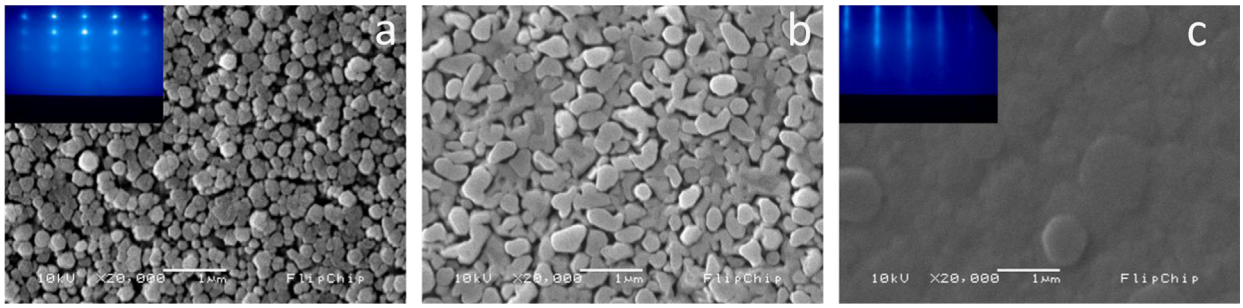

Fig. 5. $In_xGa_{1-x}N$ nanocolumn: scanning electron microscope (SEM) top view of the nanocolumns during the growth of the device. (a) InGaN:Mg nanocoulumns, (b) start of the GaN:Mg nanocolumn coalescence, (c) fully coalesced GaN:Mg cap layer.

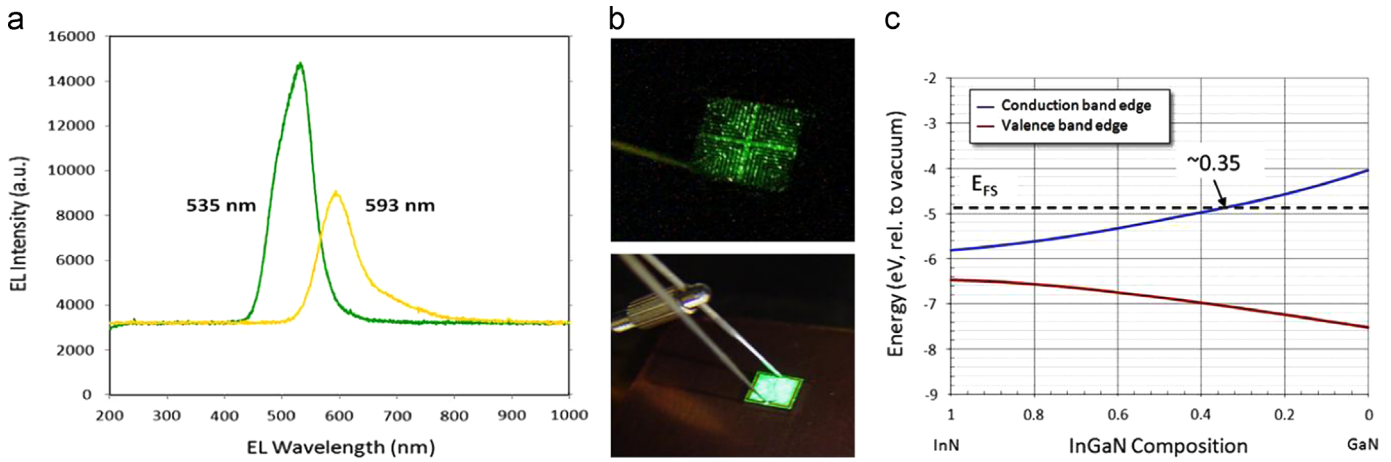

Fig. 6. $In_xGa_{1-x}N$ nanocolumn LEDs: (a) electroluminescence at room temperature, (b) low current and high current optical view of a 5×5 mm LED, (c) energy with respect to vacuum of the conduction and valence band edges, as a function of $In_xGa_{1-x}N$ composition.

Two different samples have been used to measure the electroluminescence. The EL intensity for the two structures is presented in Fig. 6(a). In Fig. 6(b) the emission of large area (5×5) mm, green LED is presented at low and high current. At low current the columnar emitters are visible (top).

Although the current injection characteristics were the same for the two structures, it is noticeable that the intensity of the yellow LED is reduced by almost 40% when compared to the intensity of the green LED. The decrease of the emission intensity has been known to occur in correlation with the increase of the indium fraction in the quantum wells of the GaN/InGaN LEDs [11].

While most of the work has been focused toward the mitigation of the carrier separation in the quantum wells (QCSE), the reduction of the polarization through the use of non-polar substrates has not provided the desired advance. More recently, the use of strain compensation techniques have allowed the achievement of larger than 1 W light power output [12]. However, the external quantum efficiency for these structures has remained below 3% demonstrating the conversion process inefficiency.

It has been demonstrated that the density of the threading dislocations is a factor in the degradation of the light emission efficiency in GaN [13]. The resilience of the III-nitrides to the presence of dislocations with densities in the range from $10^8\ cm^{-2}$ to $10^{10}\ cm^{-2}$ is due in large part to the potential barriers separating the surface of these dislocations from the bulk of the semiconductor volume, either n-doped or p-doped. Excited carriers can overcome the barriers ($E_e = 0.55$ eV, $E_h = 0.9$ eV) under light excitation and this behavior has been manifested and studied as photoconductivity. The presence of external bias and injection charges at the surface of the dislocations can also alter the band bending and the width of the barrier. However, the strongest effect on the barrier height is associated with the increase of indium fraction in InGaN, as can be seen from Fig. 6(c). In n-type GaN the conduction band edge is pinned above the Fermi stabilization level (E_{FS}) and a thin region at the surface is depleted from electrons [14]. The increase of the indium fraction reduces gradually the barrier height such as at ~35% indium fraction the relative energy of the conduction band coincides with the Fermi stabilization level and the flat band condition is reached. For InGaN with indium fractions larger than 35% the conduction band edge is pinned below the Fermi level (E_{FS}), allowing electrons to accumulate at the material surface.

We speculate that this gradual reduction of the potential barrier at the InGaN surface is responsible for the increase of the leakage currents in InGaN p–n junctions and is the mechanism that governs the gradual reduction in the external quantum efficiency of the light emitting diodes (LEDs) with the increase of the indium fraction in the active region. This phenomenon is also known as the "Green Gap". The emission wavelength corresponding to 35% indium fraction is ~583 nm, located in the yellow band of the visible spectrum.

4. Concluding remarks

The quantitative limits of Mg and Ge doping of GaN and InGaN have been explored and the effect of impurity incorporation has been evaluated with respect to the impact on material crystalline quality, carrier mobility and carrier density. For the case of InGaN, the competition between In and Mg determines the upper limit for p-type doping. We have found that for Mg fluxes larger than 1×10^{-7} Torr (BEP) corresponding to Mg volume density of more than $3 \times 10^{21}\ cm^{-3}$ indium incorporation has been largely prevented.

InGaN nanocolumn p–n junctions were grown on silicon (1 1 1) using a buffer layer of n-AlN/n-GaN and p-GaN as cap layer. The p–n junction were located in the InGaN column volume. The coalescence of the p-GaN layer has been successfully employed for the separation of the metal deposition from the p–n junction region. The electroluminescence of these structures has been measured with wavelengths of 535 nm (green) and 593 nm (yellow). The intensity of the yellow LED has shown a decrease of almost 40% when compared with that of the green LED.

We propose that the EQE decrease associated with the increase of the In fraction in the active region of LEDs, known as the "Green Gap", is determined by the decrease of the energy barrier separating the surface of threading dislocations from the volume of the semiconductor structure. Our assertion is based on indirect evidence obtained performing photovoltaic experiments and on the calculated position of the band gap edges with respect to Fermi stabilization energy.

Acknowledgements

This work was supported by RoseStreet Energy Laboratory, Contract LB07003462 and U.S. DOD/DARPA under contract W91CRB-11-C-0012.

References

[1] J. Wu, W. Walukiewicz, K.M. Yu, W. Shan, J.W. Ager III, E.E. Haller, H. Lu, W. J. Schaff, W.K. Metzger, S. Kurtz, J. Appl. Phys. 94 (2003) 6477.

[2] I. Gherasoiu, L.A. Reichertz, K.M. Yu, J.W. Ager III, V.M. Kao, W. Walukiewicz, Phys. Status Solidi C 8 (7–8) (2011) 2466–2468.

[3] I. Gherasoiu, K.M. Yu, L.A. Reichertz, V.M. Kao, M. Hawkridge, J.W. Ager III, W. Walukiewicz, Phys. Status Solidi B 247 (7) (2010) 1747–1749.

[4] S. Li, A. Waag, J. Appl. Phys. 111 (2012) 071101.

[5] L.-Y. Chen, Y.-Y. Huang, C.-S. Chang, J.J. Huang, in: Proceedings of the CS MANTECH Conference, Portland, Oregon, USA, May 17th-20th, 2010.

[6] A. Kikuchi, M. Tada, K. Miwa, K. Kishino, in: Proceedings of SPIE, Vol. 6129, 2006, 612905.

[7] I. Gherasoiu, K.M. Yu, L.A. Reichertz, W. Walukiewicz, Phys. Status Solidi C 11 (3–4) (2014) 381–384.

[8] M.A. Reshchikov, D.O. Demchenko, J.D. McNamara, S. Fernandez-Garrido, R. Calarco, Phys. Rev. B 90 (2014) 035207.

[9] M.A. Reshchikova, H. Morkoç, J. Appl. Phys. 97 (2005) 061301.

[10] C.T. Foxon, S.V. Novikov, J.L. Hall, R.P. Campion, D. Cherns, I. Griffiths, S. Khongphetsak, J. Cryst. Growth 311 (2009) 3423.

[11] C. Wetzel, M. Zhu, Y. Li, W. Hou, L. Zhao, W. Zhao, S. You, C. Stark, Y. Xia, M. DiBiccari, T. Detchprohm, in: Proceedings of the SPIE 7422, Ninth International Conference on Solid State Lighting, August 18, 2009. http://dx.doi.org/10.1117/12.829513, 742204.

[12] Shinji Saito, Rei Hashimoto, Jongil Hwang, Shinya Nunoue, Applied Physics Express 6 (11) (2013) 111004.

[13] Sergey Yu. Karpov, Yuri N. Makarov, Appl. Phys. Lett. 81 (23) (2002) 4721–4723.

[14] S.X. Li, K.M. Yu, J. Wu, R.E. Jones, W. Walukiewicz, J.W. Ager III, W. Shan, E. E. Haller, Hai Lu, William J. Schaff, Phys. Rev. B 71 (R) (2005) 161201.